Supporting Information

Evidence of multiple sorption modes in layered double hydroxides using Mo as structural probe

Bin Ma[*,a], Alejandro Fernandez-Martinez[a], Sylvain Grangeon[b], Christophe Tournassat[b], Nathaniel Findling[a], Francis Claret[b], Ayumi Koishi[a], Nicolas C. M. Marty[b], Delphine Tisserand[a], Sarah Bureau[a], Eduardo Salas-Colera[c,d], Erik Elkaïm[e], Carlo Marini[f], Laurent Charlet[a]

[a] Université Grenoble Alpes, CNRS, ISTerre, F-38041 Grenoble, France.

[b] BRGM, 3 Avenue Guillemin, Orléans Cedex 2, 45060, France.

[c] Instituto de Ciencia de Materiales de Madrid, CSIC, Sor Juana Inés de la Cruz 3, 28049, Cantoblanco Madrid, Spain.

[d] Spanish CRG BM25 SpLine Beamline at the ESRF, 71 Avenue de Martyrs, F-38043 Grenoble, France.

[e] Synchrotron SOLEIL, l'Orme des Merisiers Saint-Aubin, 91192 Gif-sur-Yvette Cedex, France

[f] CELLS-ALBA, Carretera B.P. 1413, Cerdanyola del Vallès, 08290 Barcelona, Spain

The Supporting Information contains 21 pages, 2 texts, 7 tables and 13 figures.

Text S1. Characterization of Synthesized CaAl LDHs.

Freshly synthesized Cl^- and SO_4^{2-} CaAl LDHs have well-crystallized hexagonal-shaped plate morphology (Figure S2) but different average sizes: around Ø0.5 µm for AFm-Cl_2 and Ø5 µm AFm-SO_4, respectively. The specific surface areas and the average edge lengths thus differ (Table S6), with lateral surface (S_l) area concentrations equal for AFm-Cl_2 and AFm-SO_4 to 2.19×10^{18} and 2.29×10^{17} nm^2 g^{-1}, respectively, as obtained from[1]:

$$S_l = \frac{P}{S \times \rho} \quad (1)$$

where P, S, and ρ represent CaAl LDHs particle's perimeter (nm), basal plane surface area (nm^2), and density (g nm^{-3}), respectively.

X-ray diffraction (XRD) was used to determine the nature and amount of eventual impurities and the inter-layer distances of the synthesized CaAl LDHs (Figure S1), including AFm-SO_4, AFm-Cl_2, and AFm-CO_3. Due to the sulfate-deficiency during the synthesis, no ettringite was formed in the fresh AFm-SO_4, but katoite [$Ca_3Al_2(OH)_{12}$] was observed as an impurity. AFm-SO_4 and AFm-Cl_2 powders were also characterized after 7 days in equilibrium with N_2-saturated water at pH 12.4. The (003) inter-layer distance of AFm-SO_4, was initially 8.128±0.006 Å at 5% relative humidity (RH) corresponding to 10.5 H_2O hydration state[2], and it changed to a shorter distance of 7.884±0.006 Å with time. The lack of SO_4^{2-} is compensated with OH^- in the inter-layer space, resulting in the formation of AFm-OH with 13 H_2O molecules[2]. Besides, a tiny diffraction peak occurred at 11.65° after equilibration of AFm-SO_4 in water, which is probably derived from gypsum formed during sample drying. A strict N_2 protection gives us confidence to exclude formation of AFm-CO_3 (i.e., CO_2 contamination) in both reacted AFm-SO_4 and AFm-Cl_2. No detectable impurity is observed with the AFm-Cl_2 phase, characterized by an inter-layer distance of 7.838±0.006 Å.

Atomic ratios between each element in CaAl LDHs were estimated by digesting 100 mg CaAl LDHs solid phase in a certain amount of 1% HNO_3, and by measuring total aqueous Ca, Al, and S concentrations using inductively coupled plasma optical emission spectrometry (ICP-OES). This nitrolysis method was applied for each CaAl LDH in duplicate. Katoite impurity in AFm-SO_4 was inferred from the Ca/Al stoichiometry. Structural water content was determined by thermal gravimetric analysis (TGA) and derivative thermogravimetric analysis (DTG) curves (Figure S9) and dehydration and dehydroxylation were included in the total water loss till 700 °C[3], at which temperature the water loss is assumed to be completed. Based on the calculation, 78 at.% AFm-SO_4 and 22 at.% katoite composed the product for AFm-SO_4 synthesis. The experimental chemical formula of AFm-SO_4 and AFm-Cl_2 were $Ca_4Al_2O_6(SO_4)_{0.92}(OH)_{0.08}\cdot 6.4H_2O$ and $Ca_4Al_2O_6Cl_{1.64}(OH)_{0.36}\cdot 7.4H_2O$, respectively.

Text S2. Instability of CaAl LDHs in presence of Mo.

The released Cl^- is more than the stoichiometric amount that may be derived from the corrosion of double-layer structure. This is confirmed by the newly appearance of a katoite diffraction peak for Mo-reacted samples in the synchrotron based XRD patterns since sample ClA (Figure S8), in agreement with saturation index (SI) computed from the aqueous phase composition after reaction of both CaAl LDHs with molybdate for 48 h (Figure S10). Molybdate could also affect heavily the metastability of AFm-SO_4 and result in ettringite formation (Figure S8). Compared to the dissolution products for 7 days (Figure S1), phases transformation seems to be promoted under the effect of molybdate. Indeed, the pair distribution function (PDF) analysis of high energy XRD data conducted on six selected sorption products, and compared to the calculated PDF patterns of katoite, ettringite, and powellite, shows almost no apparent phase transformation, except the formation of katoite and ettringite in Mo-reacted AFm-Cl_2 and AFm-SO_4, respectively (Figure S11 and Figure S12).

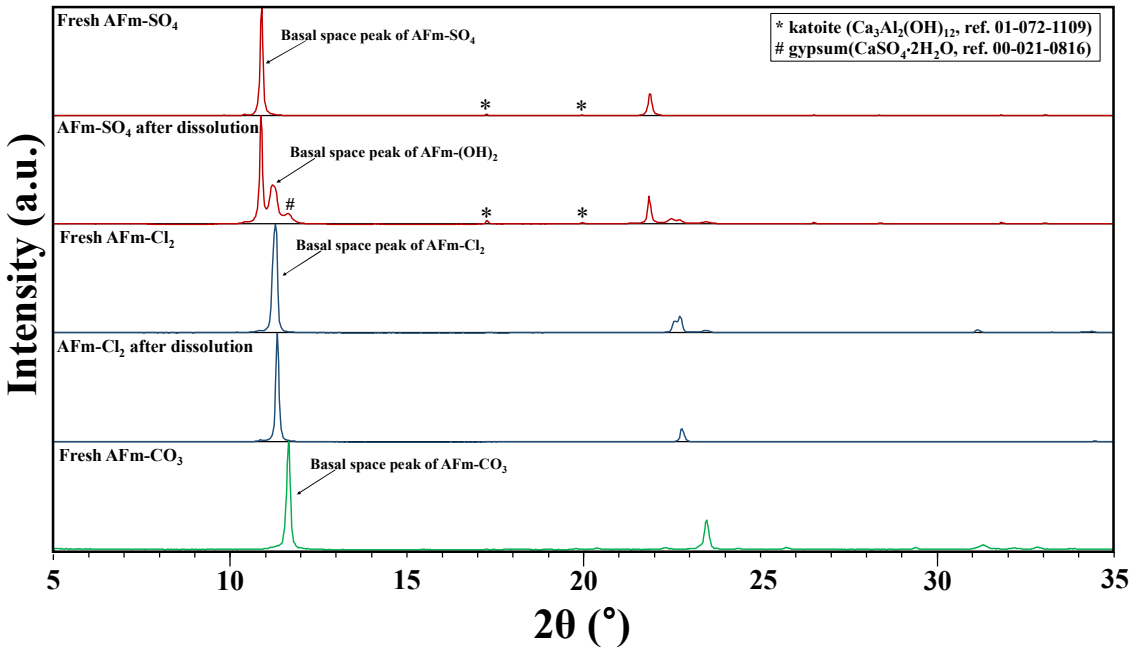

Figure S1. X-ray diffraction patterns of fresh CaAl LDHs and the phases after dissolution. The dissolution equilibrium was set at pH ~12.4 for 7 days and samples were mounted oriented at relative humidity of 5%. Cu Kα radiation at 1.5406 Å is used.

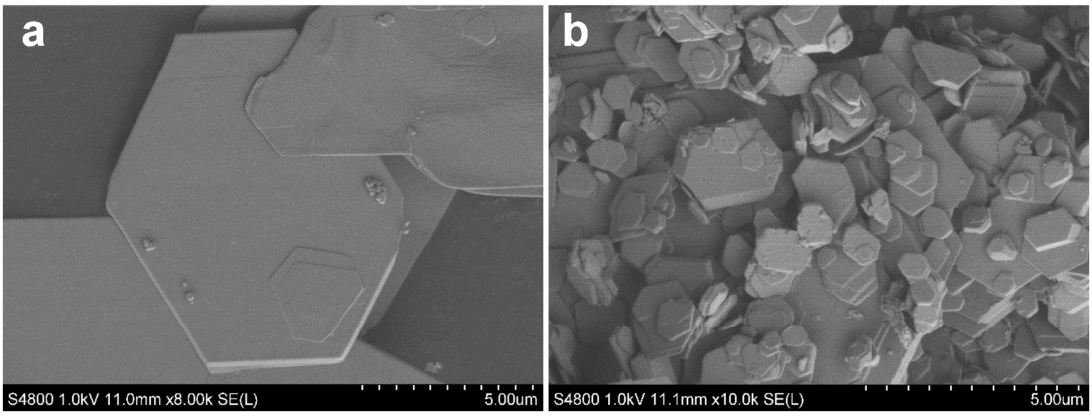

Figure S2. FE-SEM micrographs of the synthesized CaAl LDHs. Scale bar, 5 μm. (a) Pristine AFm-SO_4 particles. (b) Pristine AFm-Cl_2 particles.

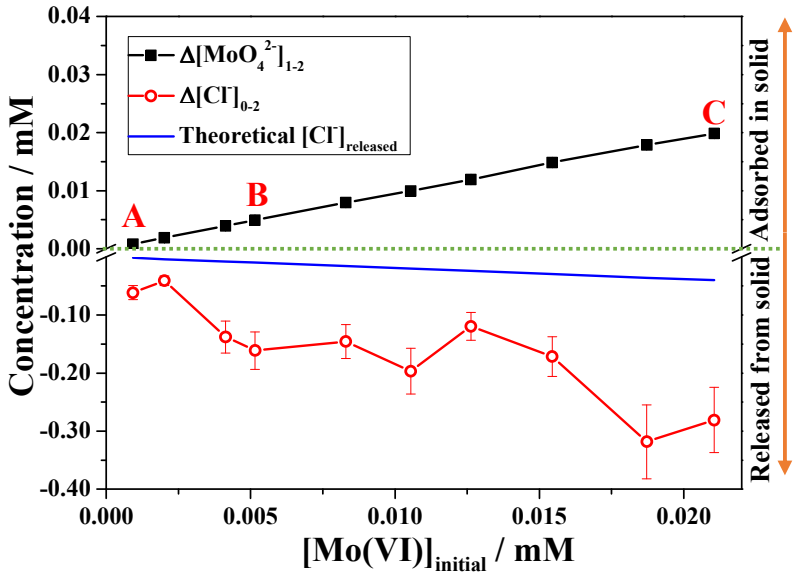

76

77 **Figure S3.** Concentration variation profile of aqueous MoO_4^{2-} and Cl^- as a function of

78 molybdate loading on AFm-Cl_2. The change in concentration of adsorbed MoO_4^{2-} is plotted

79 by the black solid dots and the released Cl^- is represented by the red hollow dots. The

80 theoretical $[Cl^-]_{released}$ is estimated by a stoichiometric anion exchange, shown as the blue

81 curve. The selected three adsorption products are marked by A, B, and C.

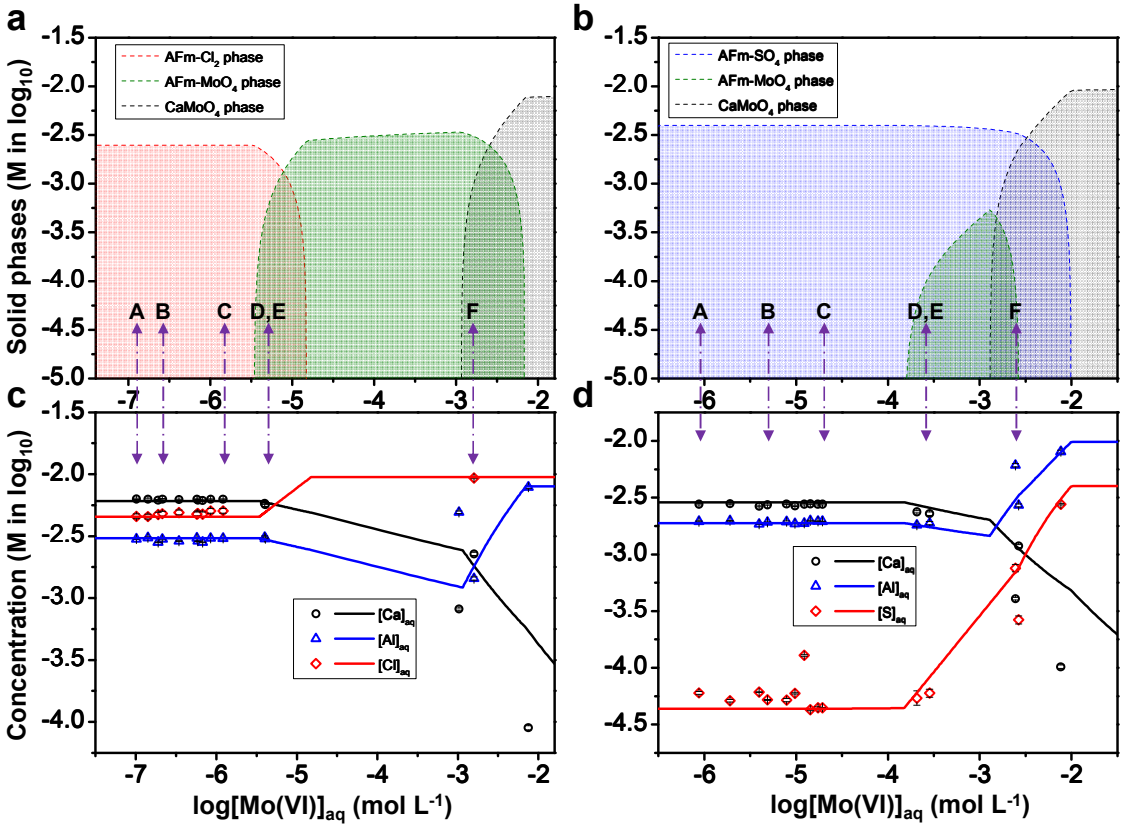

82

83 **Figure S4.** PHREEQC modelling results as a function of $[Mo(VI)]_{aq}$ in equilibrium. (a)

84 Dominated solid speciation in AFm-Cl_2 reactors. (b) Dominated solid speciation in AFm-SO_4

85 reactors. (c) Modelling results of aqueous Ca, Al, and Cl concentrations in AFm-Cl_2 reactors.

86 (b) Modelling results of aqueous Ca, Al, and S concentrations in AFm-SO_4 reactors. Reactors,

87 marked by A to F, correspond to the same ones in Figure 1.

88

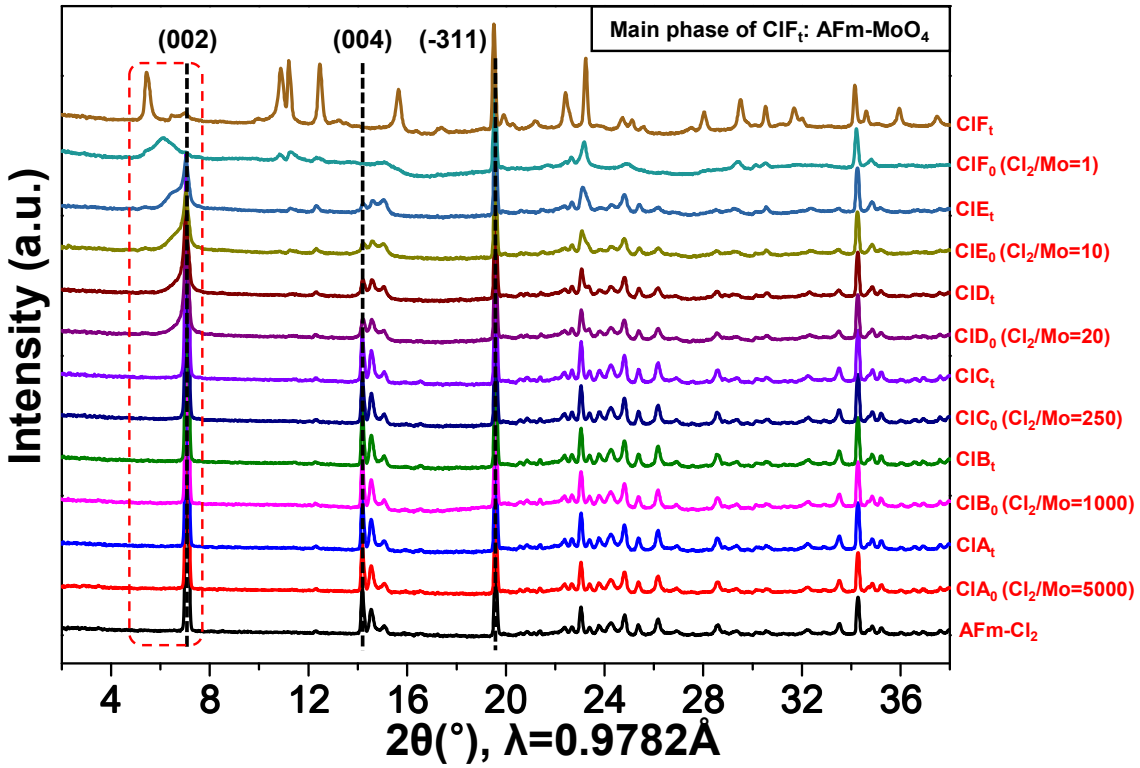

Figure S5. In-situ time resolved XRD patterns of reacted AFm-Cl_2 at each loading step. The diffraction peak range of layer-to-layer distance (d_{002}), circled by red dotted lines, is enlarged in the main text to provide more details. The Cl_2/MoO_4 ratio at each step is shown following the sample name. The main phase of ClF_t is AFm-MoO_4, with no obvious signal of katoite and powellite observed.

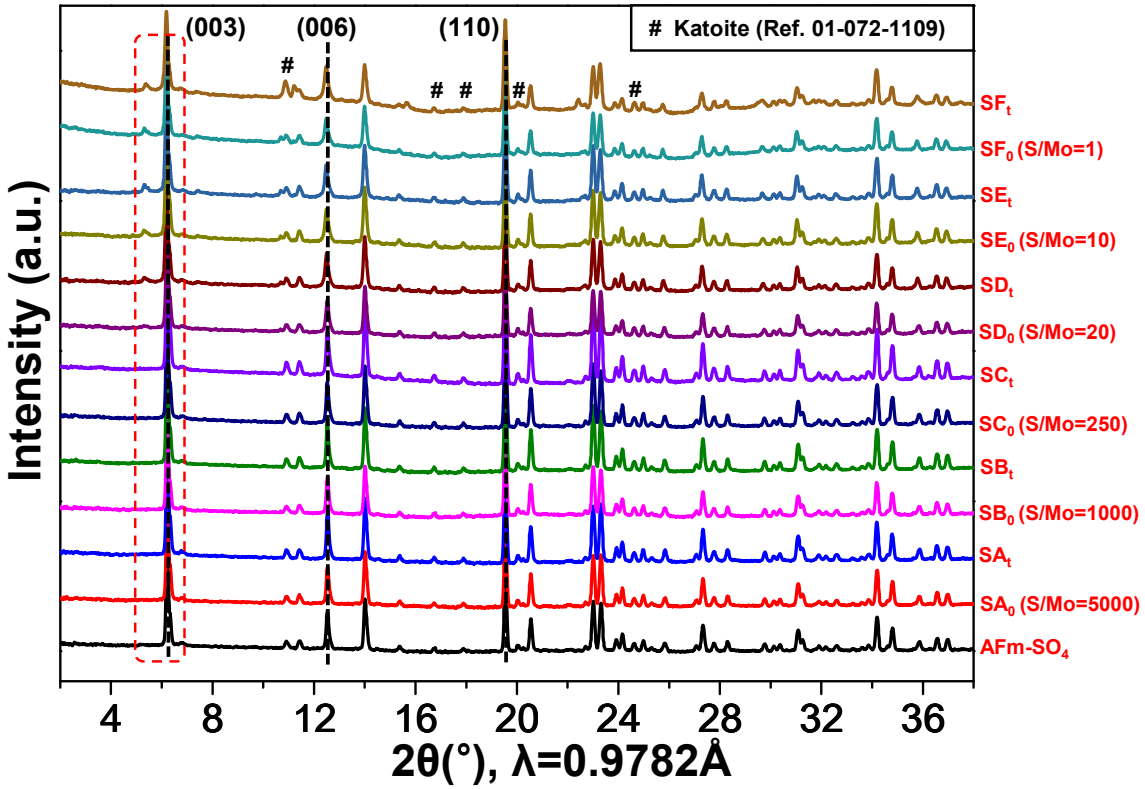

Figure S6. In-situ time resolved XRD patterns of reacted AFm-SO_4 at each loading step. The diffraction peak range of layer-to-layer distance (d_{003}), circled by red dotted lines, is enlarged in the main text to provide more details. The SO_4/MoO_4 ratio at each step is shown following the sample name.

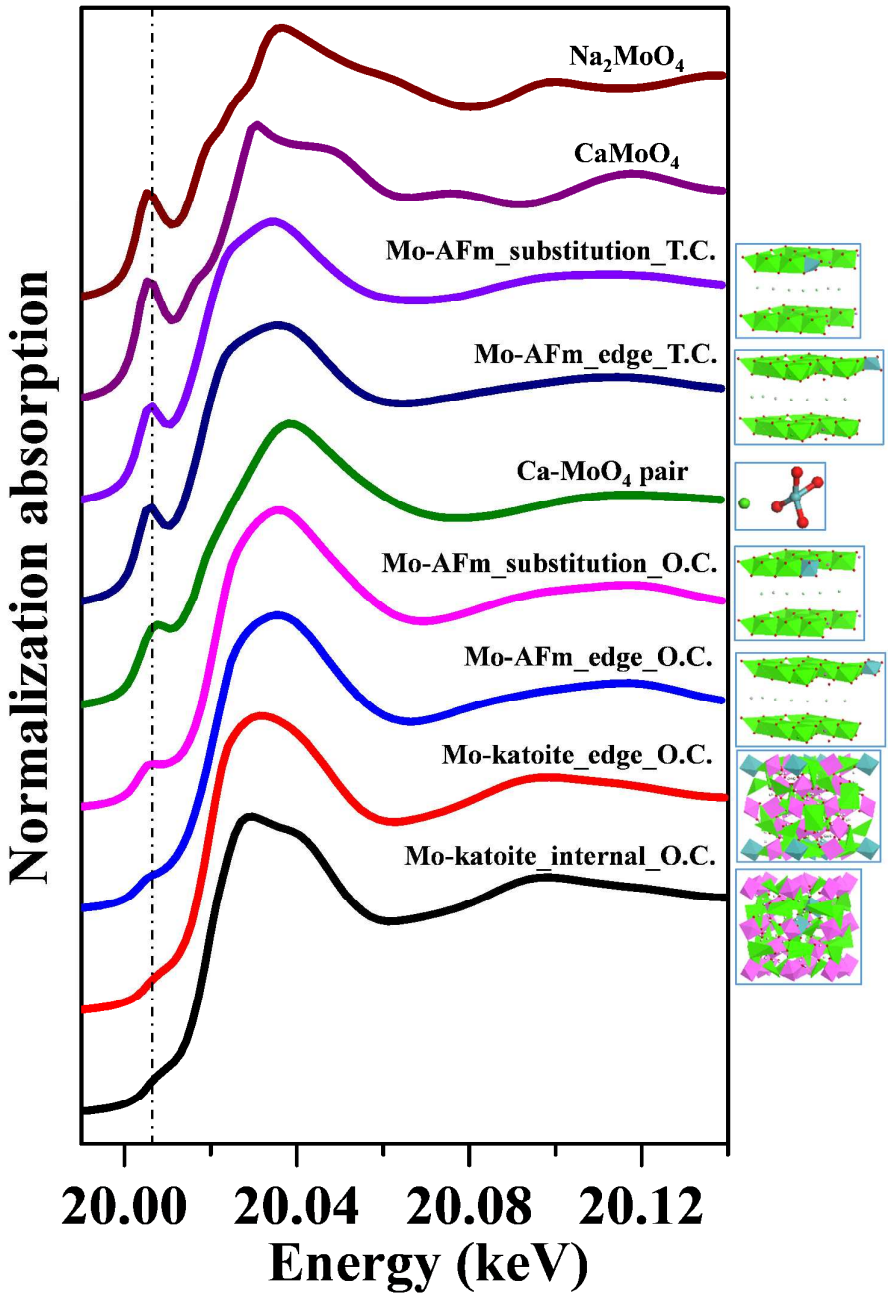

104

105 **Figure S7.** Calculated Mo K-edge XANES spectra of different Mo coordination. From the
106 bottom up, the pre-edge intensity decreases steadily and the molybdate coordination
107 environments are pure O.C. (octahedral Mo(VI)-katoite, both inner-incorporated and edge-
108 incorporated), distorted O.C. (octahedral Mo(VI)-AFm phases, both the substitution and
109 epitaxial growth), distorted T.C. (Ca-MoO_4 ion pair, both the substitution and epitaxial

growth for tetrahedral Mo(VI)-AFm phases), and pure T.C. ($CaMoO_4$ and Na_2MoO_4). O.C and T.C. represent octahedral coordination and tetrahedral coordination, respectively.

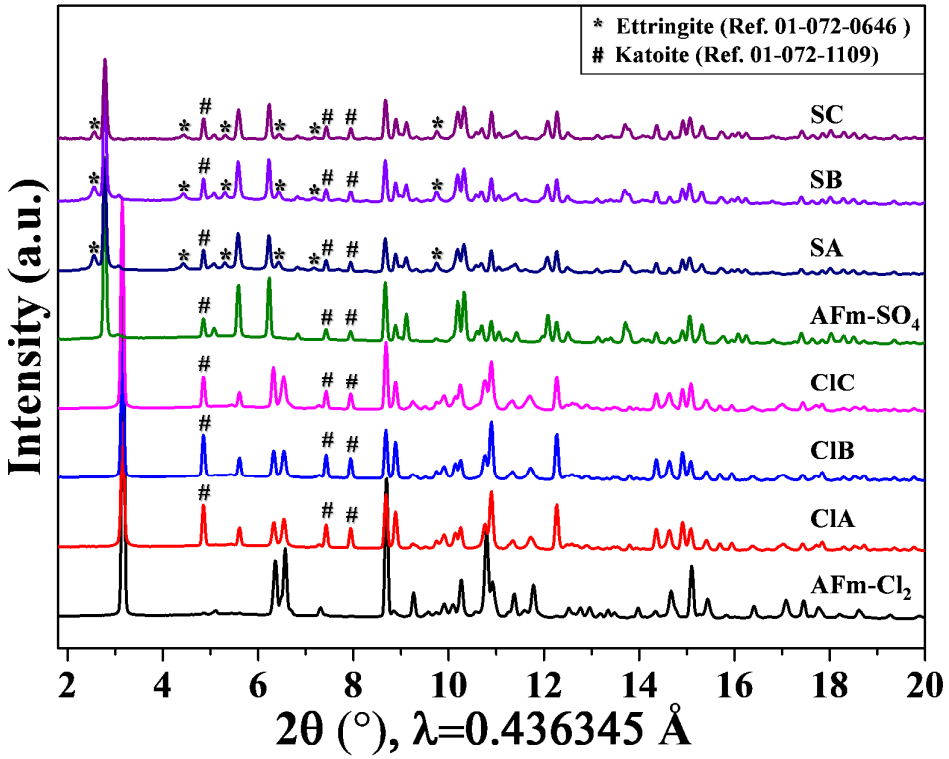

Figure S8. Synchrotron based X-ray diffraction patterns of the selected adsorption products for CaAl LDHs. Inter-layer peaks are located in the range of 2 - 4°.

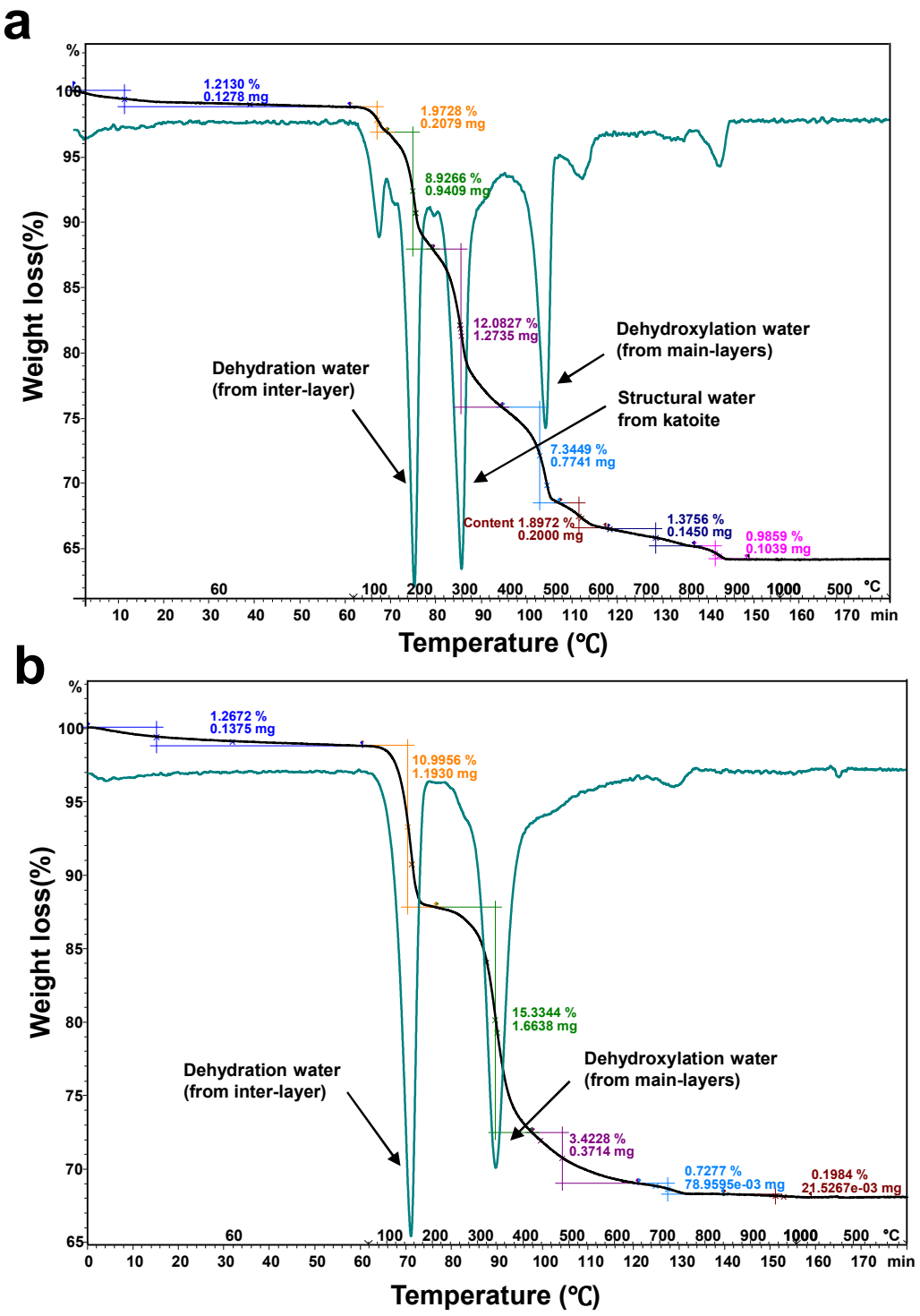

Figure S9. Thermogravimetric analyses of the synthesized CaAl LDHs. (a) AFm-SO_4 phase. (b) AFm-Cl_2 phase. TGA is represented as the black curves and DTG in olive-green curves.

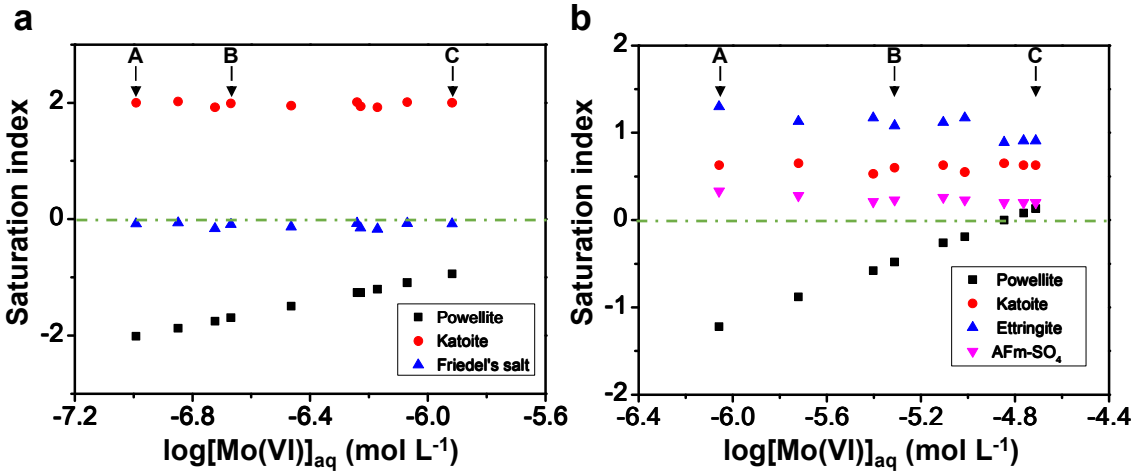

124

125 **Figure S10.** Saturation index of several possibly formed mineral phases as a function of

126 $[Mo(VI)]_{initial}$. (a) For AFm-Cl_2 system. (b) For AFm-SO_4 system. Calculation is based on the

127 aqueous data in batch sorption experiment on CaAl LDHs.

128

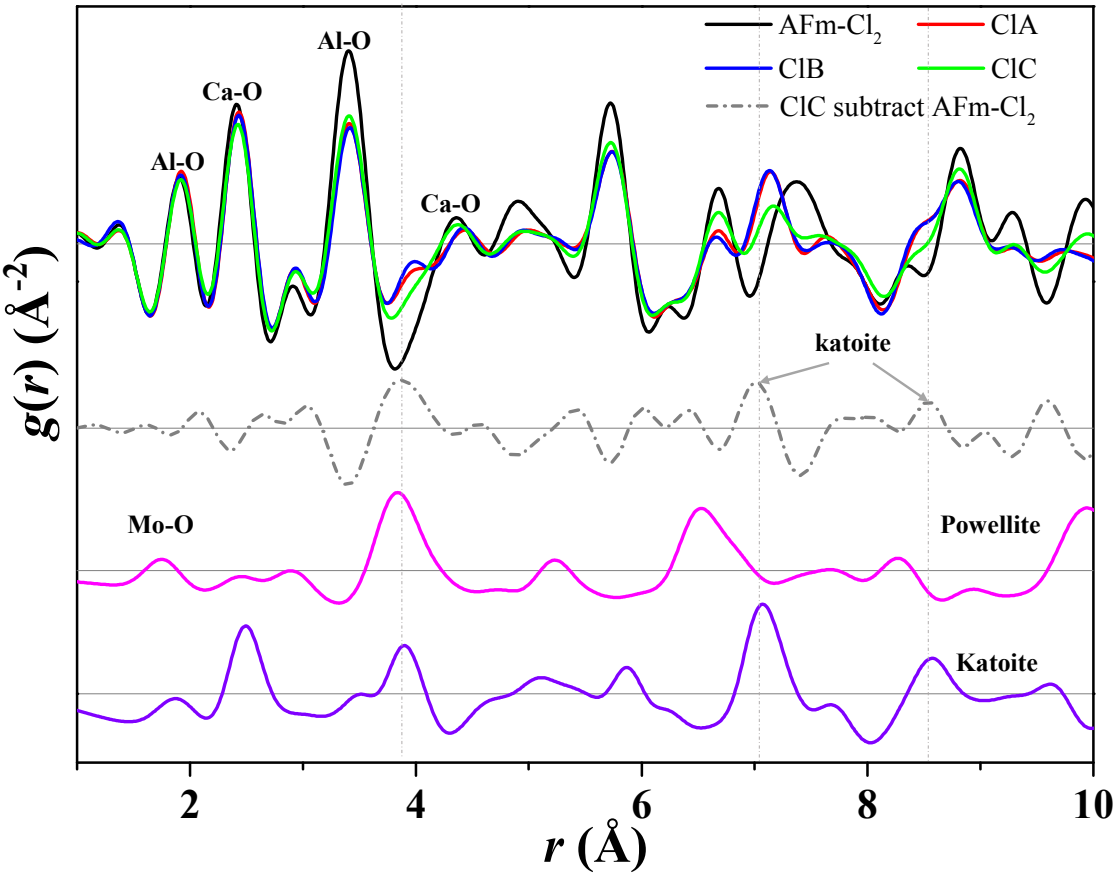

129

130 **Figure S11.** Comparison of calculated and experimental PDF of katoite, powellite, and AFm-

131 Cl_2 samples in batch sorption experiment. The grey dotted line is the subtracted signal of ClC

132 on fresh AFm-Cl_2.

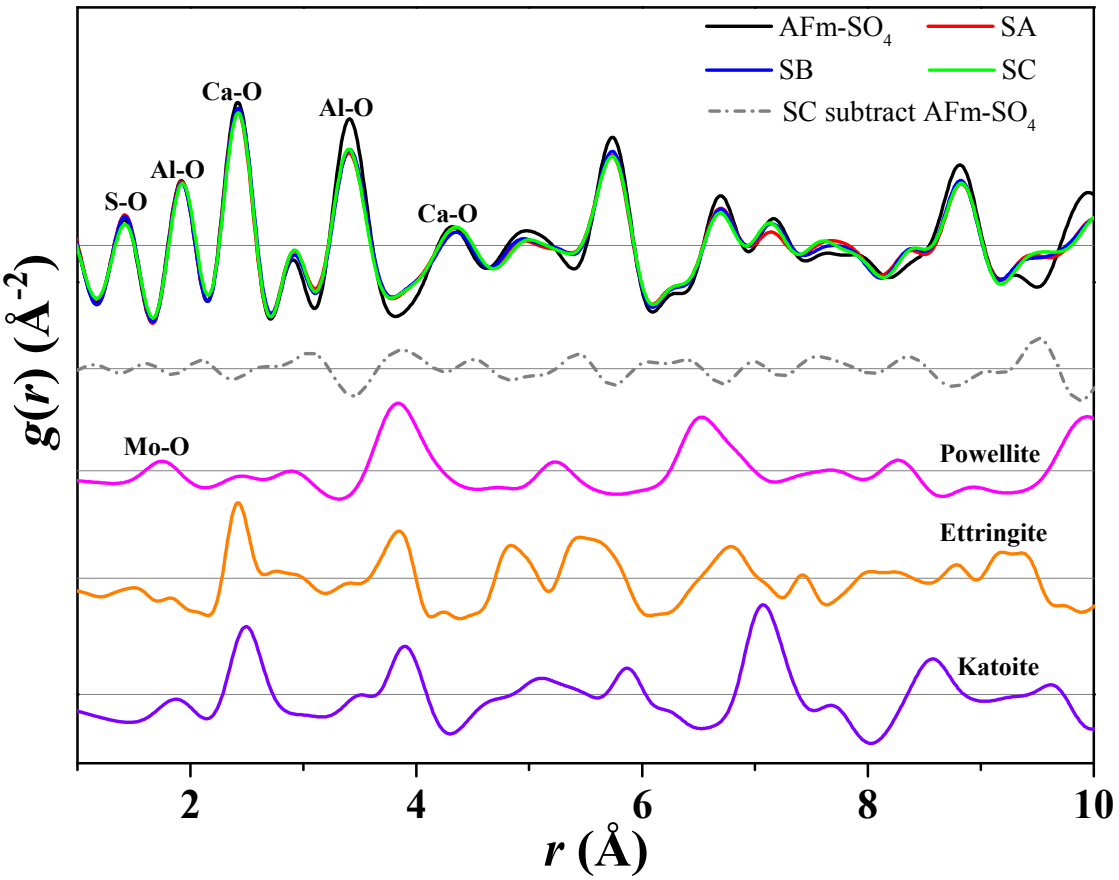

133

134 **Figure S12.** Comparison of calculated and experimental PDF of katoite, powellite, ettringite

135 and AFm-SO_4 samples in batch sorption experiment. The grey dotted line is the subtracted

136 signal of SC on fresh AFm-SO_4.

137

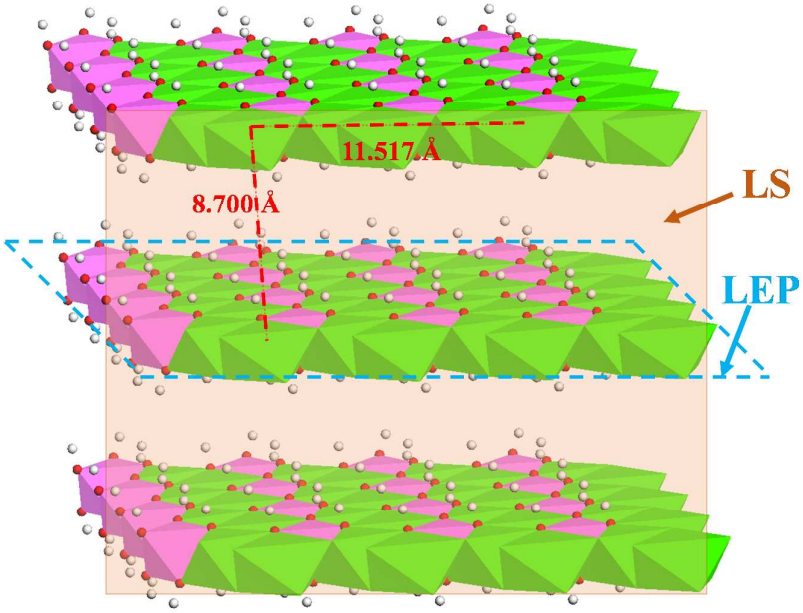

Figure S13. Schematic representation of the meaning of LS and LEP in LDHs. LS and LEP represent lateral surface and lateral edge perimeter, respectively.

Table S1. Solution content of selected elements for AFm-Cl_2 experiments before introducing MoO_4^{2-}. Concentrations were determined after reaching dissolution equilibrium, which was confirmed by dissolution kinetics[a].

ID	pH	$[Ca]_{aq}$ /mol L^{-1}	$[Al]_{aq}$ /mol L^{-1}	$[Cl]_{aq}$ /mol L^{-1}
ClA	12.37	$6.23(6)\times10^{-3}$	$3.25(1)\times10^{-3}$	$4.49(21)\times10^{-3}$
	nd	$6.31(7)\times10^{-3}$	$3.25(2)\times10^{-3}$	$4.54(21)\times10^{-3}$
	nd	$6.43(7)\times10^{-3}$	$3.25(2)\times10^{-3}$	$4.59(22)\times10^{-3}$
ClB	nd	$6.24(7)\times10^{-3}$	$3.26(2)\times10^{-3}$	$4.64(21)\times10^{-3}$
	nd	$6.36(8)\times10^{-3}$	$3.22(2)\times10^{-3}$	$4.76(23)\times10^{-3}$
	nd	$6.31(7)\times10^{-3}$	$3.29(3)\times10^{-3}$	$4.63(21)\times10^{-3}$
	nd	$6.35(6)\times10^{-3}$	$3.29(3)\times10^{-3}$	$4.64(23)\times10^{-3}$
	nd	$6.26(7)\times10^{-3}$	$3.24(1)\times10^{-3}$	$4.58(22)\times10^{-3}$
	nd	$6.28(6)\times10^{-3}$	$3.27(2)\times10^{-3}$	$4.74(21)\times10^{-3}$
ClC	nd	$6.28(6)\times10^{-3}$	$3.27(1)\times10^{-3}$	$4.79(23)\times10^{-3}$

[a] nd: not determined; Uncertainties from three times repeated analyses of identical samples are given by the number in brackets on the last digit(s).

Table S2. Solution content of selected elements for AFm-Cl_2 experiments after equilibrium with MoO_4^{2-} for 48 h[a].

ID	pH	$[Mo]_{aq}$ /mol L^{-1}	q /mol g^{-1}	$[Ca]_{aq}$ /mol L^{-1}	$[Al]_{aq}$ /mol L^{-1}	$[Cl]_{aq}$ /mol L^{-1}
ClA	12.37	$1.42(17)\times10^{-7}$	$3.93(42)\times10^{-7}$	$6.30(10)\times10^{-3}$	$3.07(4)\times10^{-3}$	$4.55(21)\times10^{-3}$
	nd	$1.02(12)\times10^{-7}$	$9.57(51)\times10^{-7}$	$6.32(8)\times10^{-3}$	$3.00(2)\times10^{-3}$	$4.58(21)\times10^{-3}$
	nd	$1.89(18)\times10^{-7}$	$1.97(13)\times10^{-6}$	$6.19(7)\times10^{-3}$	$2.82(2)\times10^{-3}$	$4.73(22)\times10^{-3}$
ClB	12.37	$2.14(8)\times10^{-7}$	$2.47(16)\times10^{-6}$	$6.29(8)\times10^{-3}$	$2.99(3)\times10^{-3}$	$4.80(22)\times10^{-3}$
	nd	$3.43(3)\times10^{-7}$	$3.98(21)\times10^{-6}$	$6.25(6)\times10^{-3}$	$2.88(1)\times10^{-3}$	$4.90(22)\times10^{-3}$
	nd	$5.91(7)\times10^{-7}$	$4.98(32)\times10^{-6}$	$6.18(6)\times10^{-3}$	$2.88(1)\times10^{-3}$	$4.83(22)\times10^{-3}$
	nd	$6.74(13)\times10^{-7}$	$5.98(30)\times10^{-6}$	$6.15(8)\times10^{-3}$	$2.82(2)\times10^{-3}$	$4.76(22)\times10^{-3}$
	nd	$5.75(16)\times10^{-7}$	$7.43(38)\times10^{-6}$	$6.28(6)\times10^{-3}$	$3.06(1)\times10^{-3}$	$4.76(22)\times10^{-3}$
	nd	$8.51(16)\times10^{-7}$	$8.93(40)\times10^{-6}$	$6.28(6)\times10^{-3}$	$3.04(1)\times10^{-3}$	$5.06(23)\times10^{-3}$
ClC	12.37	$1.21(1)\times10^{-6}$	$9.92(44)\times10^{-6}$	$6.28(6)\times10^{-3}$	$3.03(2)\times10^{-3}$	$5.07(23)\times10^{-3}$
ClD	12.38	$3.98(32)\times10^{-6}$	$1.35(4)\times10^{-4}$	$5.83(15)\times10^{-3}$	$3.10(7)\times10^{-3}$	nd
ClE	12.38	$4.05(28)\times10^{-6}$	$2.60(7)\times10^{-4}$	$5.68(19)\times10^{-3}$	$3.02(5)\times10^{-3}$	nd
ClF	12.37	$1.59(13)\times10^{-3}$	$1.52(7)\times10^{-3}$	$2.27(7)\times10^{-3}$	$1.44(4)\times10^{-3}$	$9.35(16)\times10^{-3}$
ClG	12.41	$1.03(5)\times10^{-3}$	$3.90(9)\times10^{-3}$	$8.15(16)\times10^{-4}$	$4.93(12)\times10^{-3}$	nd
ClH	12.42	$7.50(35)\times10^{-3}$	$6.14(21)\times10^{-3}$	$8.97(36)\times10^{-5}$	$7.86(23)\times10^{-3}$	nd

[a] nd: not determined; Uncertainties from three times repeated analyses of identical samples are given by the number in brackets on the last digit(s).

Table S3. Solution content of selected elements for AFm-SO_4 experiments before introducing MoO_4^{2-}. Concentrations were determined after reaching dissolution equilibrium, which was confirmed by dissolution kinetics[a].

ID	pH	$[Ca]_{aq}$ /mol L^{-1}	$[Al]_{aq}$ /mol L^{-1}	$[S]_{aq}$ /mol L^{-1}
SA	12.35	$2.69(3)\times10^{-3}$	$1.97(2)\times10^{-3}$	$5.08(22)\times10^{-5}$
	nd	$2.74(4)\times10^{-3}$	$1.97(2)\times10^{-3}$	$5.32(17)\times10^{-5}$
	nd	$2.77(3)\times10^{-3}$	$1.96(1)\times10^{-3}$	$5.08(26)\times10^{-5}$
SB	nd	$2.70(3)\times10^{-3}$	$1.98(1)\times10^{-3}$	$5.13(14)\times10^{-5}$
	nd	$2.73(3)\times10^{-3}$	$1.97(2)\times10^{-3}$	$4.88(29)\times10^{-5}$
	nd	$2.74(3)\times10^{-3}$	$1.97(1)\times10^{-3}$	$4.98(24)\times10^{-5}$
	nd	$2.68(2)\times10^{-3}$	$1.89(1)\times10^{-3}$	$6.04(16)\times10^{-5}$
	nd	$2.71(3)\times10^{-3}$	$1.96(1)\times10^{-3}$	$5.00(5)\times10^{-5}$
	nd	$2.72(3)\times10^{-3}$	$1.95(2)\times10^{-3}$	$4.93(24)\times10^{-5}$
SC	nd	$2.74(3)\times10^{-3}$	$1.97(2)\times10^{-3}$	$5.02(44)\times10^{-5}$

[a] nd: not determined; Uncertainties from three times repeated analyses of identical samples are given by the number in brackets on the last digit(s).

Table S4. Solution content of selected elements for AFm-SO_4 experiments after equilibrium with MoO_4^{2-} for 48 h[a].

ID	pH	$[Mo]_{aq}$ /mol L^{-1}	q /mol g^{-1}	$[Ca]_{aq}$ /mol L^{-1}	$[Al]_{aq}$ /mol L^{-1}	$[S]_{aq}$ /mol L^{-1}
SA	12.34	$8.75(90)\times10^{-7}$	$2.62(3.04)\times10^{-8}$	$2.77(3)\times10^{-3}$	$1.95(2)\times10^{-3}$	$6.00(17)\times10^{-5}$
	nd	$1.90(11)\times10^{-6}$	$5.61(3.67)\times10^{-8}$	$2.80(3)\times10^{-3}$	$1.97(2)\times10^{-3}$	$5.11(13)\times10^{-5}$
	nd	$3.96(26)\times10^{-6}$	$8.76(9.20)\times10^{-8}$	$2.65(3)\times10^{-3}$	$1.85(1)\times10^{-3}$	$6.09(4)\times10^{-5}$
SB	12.35	$4.88(35)\times10^{-6}$	$1.39(1.18)\times10^{-7}$	$2.74(3)\times10^{-3}$	$1.92(1)\times10^{-3}$	$5.21(4)\times10^{-5}$
	nd	$7.86(49)\times10^{-6}$	$2.21(1.59)\times10^{-7}$	$2.78(4)\times10^{-3}$	$1.94(3)\times10^{-3}$	$5.19(17)\times10^{-5}$
	nd	$9.70(6)\times10^{-6}$	$4.22(2.25)\times10^{-7}$	$2.68(3)\times10^{-3}$	$1.86(1)\times10^{-3}$	$5.95(9)\times10^{-5}$
	nd	$1.23(8)\times10^{-5}$	$1.85(2.20)\times10^{-7}$	$2.77(4)\times10^{-3}$	$1.88(3)\times10^{-3}$	$1.29(2)\times10^{-4}$
	nd	$1.43(8)\times10^{-5}$	$5.89(2.84)\times10^{-7}$	$2.79(4)\times10^{-3}$	$1.98(2)\times10^{-3}$	$4.27(9)\times10^{-5}$
	nd	$1.73(6)\times10^{-5}$	$7.29(2.58)\times10^{-7}$	$2.77(4)\times10^{-3}$	$1.96(2)\times10^{-3}$	$4.44(9)\times10^{-5}$
SC	12.34	$1.94(5)\times10^{-5}$	$8.17(2.51)\times10^{-7}$	$2.77(3)\times10^{-3}$	$1.95(1)\times10^{-3}$	$4.45(3)\times10^{-5}$
SD	12.35	$2.07(12)\times10^{-4}$	$3.30(49)\times10^{-5}$	$2.37(6)\times10^{-3}$	$1.81(4)\times10^{-3}$	$5.41(86)\times10^{-5}$
SE	12.36	$2.84(17)\times10^{-4}$	$1.20(8)\times10^{-4}$	$2.28(8)\times10^{-3}$	$1.88(7)\times10^{-3}$	$5.98(50)\times10^{-5}$
SF	12.41	$2.66(13)\times10^{-3}$	$9.81(72)\times10^{-4}$	$1.18(3)\times10^{-3}$	$2.71(8)\times10^{-3}$	$2.65(22)\times10^{-4}$
SG	12.40	$2.45(15)\times10^{-3}$	$3.19(10)\times10^{-3}$	$4.07(9)\times10^{-4}$	$6.10(21)\times10^{-3}$	$7.56(60)\times10^{-4}$
SH	12.42	$7.63(42)\times10^{-3}$	$6.07(22)\times10^{-3}$	$1.02(4)\times10^{-4}$	$8.04(26)\times10^{-3}$	$2.77(4)\times10^{-3}$

[a] nd: not determined; Uncertainties from three times repeated analyses of identical samples are given by the number in brackets on the last digit(s).

Table S5. Equilibrium constants of selected phases[a] and reactions occurred on CaAl LDHs at each sorption stage. *log*K values of AFm edge sites sorption and AFm-MoO_4 formation were adapted.

	Equation	*logK*
Solubility equilibrium		
AFm-Cl_2	$Ca_4Al_2Cl_2(OH)_{12}\cdot 4H_2O + 12H^+ \Leftrightarrow 4Ca^{2+} + 2Al^{3+} + 2Cl^- + 16H_2O$	74.93
AFm-SO_4	$Ca_4Al_2(SO_4)(OH)_{12}\cdot 6H_2O + 12H^+ \Leftrightarrow 4Ca^{2+} + 2Al^{3+} + SO_4^{2-} + 18H_2O$	73.07
AFm-MoO_4	$Ca_4Al_2(MoO_4)(OH)_{12}\cdot 4H_2O + 12H^+ \Leftrightarrow 4Ca^{2+} + 2Al^{3+} + MoO_4^{2-} + 16H_2O$	74.00
$CaMoO_4$	$CaMoO_{4(s)} \Leftrightarrow Ca^{2+} + MoO_4^{2-}$	-7.90
Katoite(C_3AH_6)	$Ca_3Al_2(OH)_{12} + 12H^+ \Leftrightarrow 3Ca^{2+} + 2Al^{3+} + 12H_2O$	80.32
Ettringite	$Ca_6Al_2(SO_4)_3(OH)_{12}\cdot 26H_2O + 12H^+ \Leftrightarrow 6Ca^{2+} + 2Al^{3+} + 3SO_4^{2-} + 38H_2O$	56.97
Sorption stage		
Edge sorption	$2AFm\_edge\text{-}OH + MoO_4^{2-} \Leftrightarrow (AFm\_edge)_2\text{-}MoO_4 + 2OH^-$	2.80[b], 1.05[c]
AFm-MoO_4 formation	$4Ca^{2+} + 2Al^{3+} + MoO_4^{2-} + 16H_2O \Leftrightarrow Ca_4Al_2(MoO_4)(OH)_{12}\cdot 4H_2O + 12H^+$	-74.00
$CaMoO_4$ precipitation	$Ca^{2+} + MoO_4^{2-} \Leftrightarrow CaMoO_{4(s)}$	7.90

[a] *log*K values of other phases refer to THERMOCHIMIE database[4].
[b] For edge sorption on AFm-Cl_2.
[c] For edge sorption on AFm-SO_4.

Table S6. Physical parameters of AFm particles.

	SA[1] ($m^2\ g^{-1}$)	AEL[2] (μm)	Density ($g\ cm^{-3}$)	Basal area (m^2)	LEP[3] ($nm\ g^{-1}$)	LS[4] ($nm^2\ g^{-1}$)
AFm-Cl_2	3.5	0.5	2.11	6.50×10^{-13}	2.23×10^{17}	2.19×10^{18}
AFm-SO_4	1.9	5.0	2.02	6.50×10^{-11}	2.26×10^{16}	2.29×10^{17}

[1] SA represents specific surface area measured by N_2-sorption BET.
[2] AEL represents average edge length of AFm particles measured by SEM.
[3] LEP represents lateral edge perimeter.
[4] LS represents lateral surface.

Table S7. Edge sites concentration and adsorbed anion amount.

	LEP length conc. (nm L^{-1})	LS area conc. (nm^2 L^{-1})	LEP site conc. (mol L^{-1})	LS site conc. (mol L^{-1})	Sample	Adsorbed Mo amount (mol L^{-1})
					ClA	7.86×10^{-7}
AFm-Cl_2	4.45×10^{17}	4.38×10^{18}	7.39×10^{-7}	1.94×10^{-5}	ClB	4.94×10^{-6}
					ClC	1.98×10^{-5}
					SA	5.25×10^{-8}
AFm-SO_4	3.52×10^{16}	3.57×10^{17}	5.85×10^{-8}	1.58×10^{-6}	SB	2.78×10^{-7}
					SC	1.63×10^{-6}

* The L/S ratio of 500 kg/kg was used. Layers' edge and lateral adsorption site densities are estimated as 1.00 nm^{-1} and 2.67 nm^{-2} (2.67 Ca atoms are included per area of 8.700×11.517 $Å^2$, seeing Figure S13), respectively. LS and LEP represent lateral surface and lateral edge perimeter, respectively.

References

(1) Tournassat, C.; Neaman, A.; Villiéras, F.; Bosbach, D.; Charlet, L. Nanomorphology of montmorillonite particles: Estimation of the clay edge sorption site density by low-pressure gas adsorption and AFM observations. *Am. Mineral.* **2003,** *88* (11-12), 1989-1995.

(2) Baquerizo, L. G.; Matschei, T.; Scrivener, K. L.; Saeidpour, M.; Wadsö, L. Hydration states of AFm cement phases. *Cem. Concr. Res.* **2015,** *73*, 143-157.

(3) Mesbah, A.; Rapin, J. P.; Francois, M.; Cau-dit-Coumes, C.; Frizon, F.; Leroux, F.; Renaudin, G. Crystal structures and phase transition of cementitious bi-anionic AFm-(Cl^-, CO_3^{2-}) compounds. *J. Am. Ceram. Soc.* **2011,** *94* (1), 262-269.

(4) Giffaut, E.; Grivé, M.; Blanc, P.; Vieillard, P.; Colàs, E.; Gailhanou, H.; Gaboreau, S.; Marty, N.; Made, B.; Duro, L. Andra thermodynamic database for performance assessment: ThermoChimie. *Appl. Geochem.* **2014,** *49*, 225-236.